05

Effect of temperature on magnetoimpedance in amorphous microconducts $Co_{27.4}Fe_5Ni_{43.08}B_{12.26}Si_{12.26}$

© J. Alam, M.G. Nematov, N.A. Yudanov, H. Hashim, A.S. Kurochka, A.V. Nuriev, L.V. Panina¶, V.G. Kostishin

National University of Science and Technology „MISiS“,
Moscow, Russia

¶ E-maiL: drlpanina@gmail.com

Received November 1, 2022
Revised November 10, 2022
Accepted November 10, 2022

A study of the temperature behavior of high-frequency magnetoimpedance (MI) in amorphous microcircuits in a glass shell up to the Curie temperature T_C has been carried out. Samples from the alloy $Co_{27.4}Fe_5B_{12.26}Si_{12.26}Ni_{43.08}$ with a low Curie temperature ($T_C \sim 48^\circ C$) and negative magnetostriction were used. Near T_C, the impedance curves retain their characteristic behavior for materials with circular anisotropy, but the sensitivity of MI with respect to the field decreases sharply. The change in impedance with temperature becomes significant only in the presence of an external magnetic field. With an increase in temperature from room temperature to T_C, the relative change in impedance can reach 140−275% in the frequency range 0.1−0.9 GHz and a magnetic field of ~ 10 Oe. Taking into account the location of T_C in an almost important temperature region, the results obtained are interesting for the development of miniature temperature sensors, including contactless embedded sensors.

Keywords: amorphous alloys, MI-effect, circular anisotropy, spin-orientation transition.

DOI: 10.21883/PSS.2023.02.55411.513

1. Introduction

Amorphous transition metal alloys which are produced by means of rapid solidification from the melt in the form of thin ribbons or wires are of interest being the excellent soft magnetic materials since they have magnetocrystalline anisotropy virtually close to zero. Typical compounds are $(Fe, Co, Ni)_{70-85}(Si, B)_{15-30}$ at.%, where metalloids Si and B are necessary for glass formation and amorphous structure stabilization. Detailed composition may vary widely according to certain practical tasks [1–3]. For magnetoimpedance (MI) effect, CoFe-based alloys are the most promising. These alloys, by varying Fe, Mn and Ni content, can achieve almost zero and negative magnetostriction ($\sim -10^{-7}$), i.e. can also considerably reduce the magnetoelastic anisotropy. Negative magnetostriction together with tensile stresses results in „easy-plane“ type anisotropy. External magnetic field H directed along stresses is a „hard field“, and at $H \approx H_K$ (H_K is the anisotropy field), spin-orientation transition results in a fast growth of permeability [4]. For amorphous microwires, easy magnetization direction corresponds to the azimuthal direction due to decrease in magnetic dipole energy (shape anisotropy). Such anisotropy is known as circular anisotropy. External field along the microwire axis under spin-orientation transition causes dramatic increase in circular permeability and, hence, high impedance sensitivity to magnetic field in the vicinity of H_K (up to 600%/Oe [5]).

In order to be used in sensing devices, MI characteristics shall be thermally stable [6,7]. This requires sufficiently high Curie temperature (T_C) and crystallization temperature (T_{cr}) of the utilized alloys. T_{cr} increases with metalloid content, while T_C decreases. When SiB concentration is about 25 at.%, T_C in CoFe amorphous alloys exceeds 300°C, and crystallization temperature is 500°C [1], therefore such materials are suitable for application.

Magnetoelastic anisotropy of glass-encapsulated amorphous microwires can essentially depend on temperature due to internal mechanical stress relaxation. At low magnetostriction constant, this can cause changes in magnetic structure already at approx. 40−80°C [8]. Such undesired thermal effects may be removed by annealing [9].

Several publications offered to use amorphous alloys with low T_C for sensor applications [10]. Near T_C, spontaneous polarization M_s decreases; hence, other magnetic parameters such as anisotropy and magnetostriction constants also decrease. This leads to changes in MI behavior near T_C as reported in [9,11–14] for MHz frequencies. Generally, the temperature range of practical interest does not exceed 100°C. To reduce T_C, alloys with high metalloid content may be used. However, spontaneous magnetization M_s decreases dramatically in this case. On the other hand, in Co-Fe alloys with relatively high Ni or Cr content, T_C [15,16] also decreases.

Temperature behavior of MI in GHz range in glass-encapsulated amorphous microwires made from CoFeNiBSi alloys ($T_C \sim 48^\circ C$) is addressed herein. Addition of Ni not only reduces T_C, but also causes negative magnetostriction, therefore microwires have circular anisotropy and sensitive MI.

It should be noted that the change in M_s and other parameters depending on it occurs much slower in amorphous alloys than in crystalline alloys. This facilitates smooth MI-temperature dependence which is important for the development of sensors with wide operating temperature range.

2. Materials and experimental techniques

Glass-encapsulated amorphous $Co_{27.4}Fe_5B_{12.26}Si_{12.26}Ni_{43.08}$ microwires produced by the Taylor–Ulitovsky method [17] were used. Metal core diameter is $d = 31\,\mu$m, total diameter is $D = 37\,\mu$m.

The magnetostriction constant was measured by the small-angle magnetization rotation instead of angle-method [18] and was equal to $-4.2 \cdot 10^{-7}$.

Glass-encapsulated amorphous microwires are known to demonstrate considerable temperature dependence of steady-state magnetic properties as a result of internal mechanical stress relaxation which also occurs at temperatures about 40–80°C [8,19]. To avoid thermal effects not associated with the phase transition temperature, annealing at 25 mA was carried out. The annealing details and annealing temperature determination are described in [20]. In this case, this corresponds to the annealing temperature about 230°C.

T_C was calculated according to the magnetization-temperature dependence $M(T)$ measured using a vibration magnetometer (VSM, Lake Shore series 7400). For T_C measurement, the steepest segment of curve $M(T)$ measured in low fields is extrapolated to the temperature axis. The slope is determined from the numerical estimate of the maximum derivative dM/dT.

Hysteresis loops were measured by the induction method. The system used two differential coils with inner diameter of 3 mm. The specimens were magnetized in 12.5 Oe 500 Hz field. To investigate the influence of heat on the hysteresis loops, the differential coils with the specimen were placed into a heat insulated chamber with uniform heating and switch control. For temperature measurement, a thermocouple was installed near the coil with the specimen.

MI was measured using Hewlett-Packard 8753E vector network analyzer in the frequency range from 0.1 to 1.5 GHz. SOLT (Short-Open-Load-Thru) improved calibration technique was used. The technique uses specially designed strip cells as calibration standards [21,22]. This calibration is required by the measurement method where the measured item (ferromagnetic wire) shall not be connected directly to coaxial cables. The calibrations cells were made on the basis of Rogers-RT5880 printed board with permittivity 2.2 ± 0.02, which is temperature stable up to 300°C. The measurement cell includes SMA connectors (subminiature type A), microstrip lines, microwire connected to the strips by means of conducting paint. Measurement cell and specimen resistances (DC) are independent of the temperature in the test temperature range (with accuracy to the multimeter measurement error).

Impedance spectra Z were calculated by S_{21} in a standard way using the equivalent scheme: $Z = 2Z_0(1 - S_{21})/S_{21}$, $Z_0 = 50\,\Omega$. The measurement cell was placed into the Helmholtz coil where a slowly changing magnetic field up to 45 Oe is created. Temperature measurements were carried out using the same chamber as for hysteresis loops, while the thermocouple was installed near the printed board with the specimen. Impedance measurement wire length was equal to 10 mm. Meanwhile, at frequencies around 2 GHz, the electromagnetic wavelength along the specimen is about the specimen length, and it cannot be treated as a lumpt elements. Delay time shall be considered [21]. For the purpose of this research, we were limited to frequencies up to 1.5 GHz and analyzed the real part of impedance, because the delay effects provide the maximum contribution to the imaginary part of impedance.

3. Results and discussions

Figure 1 shows magnetization-temperature dependences measured in 30 and 100 Oe fields. T_C was determined by the maximum magnetization derivative for a relatively low field of 30 Oe and was equal to (48 ± 1)°C.

3.1. Hysteresis loops

Hysteresis loops of the specimens in initial conditions and after annealing for various temperatures are shown in Figure 2. Loop shapes of both specimens for all temperatures differ negligibly. At the annealing temperatures, the magnetostriction constant does not vary, and partial relaxation of internal stresses does not lead to significant anisotropy variation because the magnetostriction constant of the initial microwire is rather high. It is assumed that temperature variation in both cases is caused by the proximity to T_C only. Inclined shape of the loop corresponds to circular anisotropy in microwires with negative magnetostriction. By linear function approximation of the magnetization variation, effective anisotropy field H_K can be assessed. At room temperature, $H_K \approx 2.2$ Oe for inital specimen and $H_K \approx 2.6$ Oe for annealed specimen. When the temperature increases, the loop shape is maintained, but the anisotropy field decreases. And remanent magnetization increases, i.e. the microwire area where the easy anisotropy axis is along the wire increases.

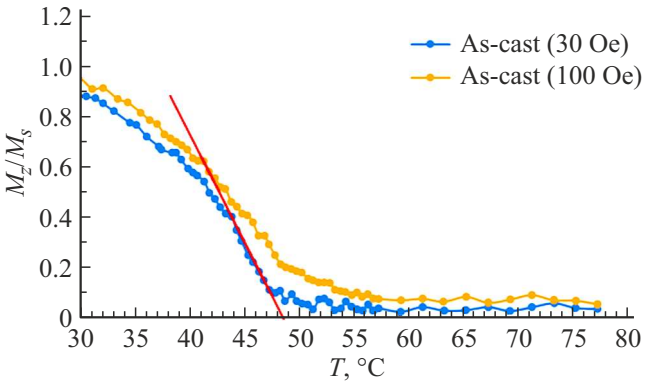

Figure 1. Temperature dependence of magnetization measured in the magnetic field along the wire (30 and 100 Oe) sufficient for saturation magnetization M_s at room temperature for initial amorphous $Co_{27.4}Fe_5B_{12.26}Si_{12.26}Ni_{43.08}$ microwire. The line corresponds to the maximum magnetization temperature-derivative.

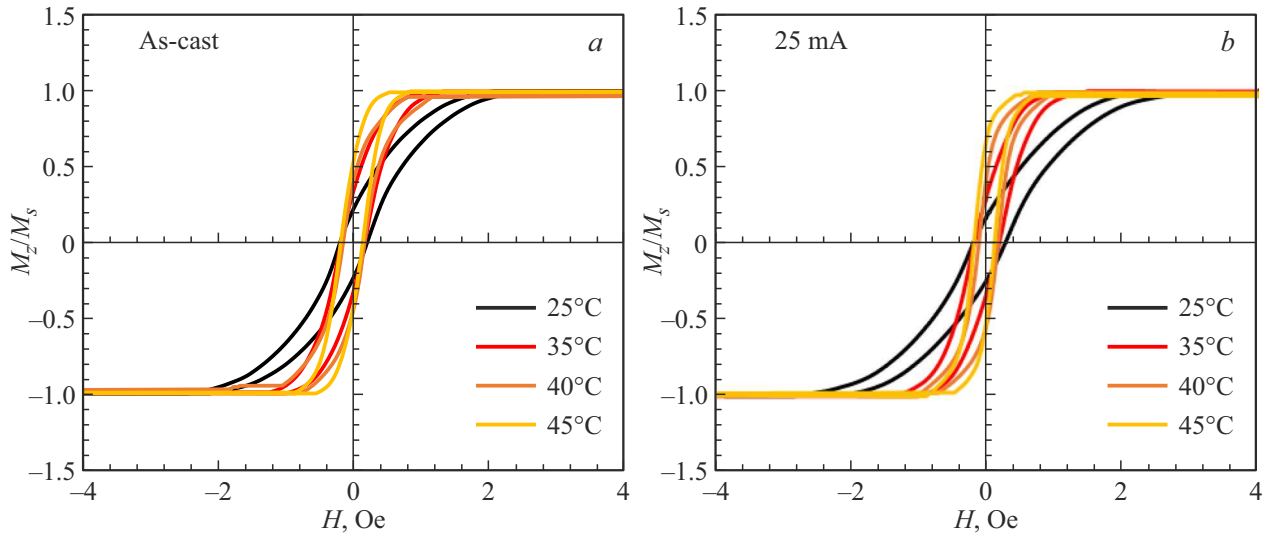

Figure 2. Hysteresis loops of $Co_{27.4}Fe_5B_{12.26}Si_{12.26}Ni_{43.08}$ microwires for various temperatures (specified for saturation magnetization at this temperature): *a* — in initial condition, *b* — after annealing at 25 mA.

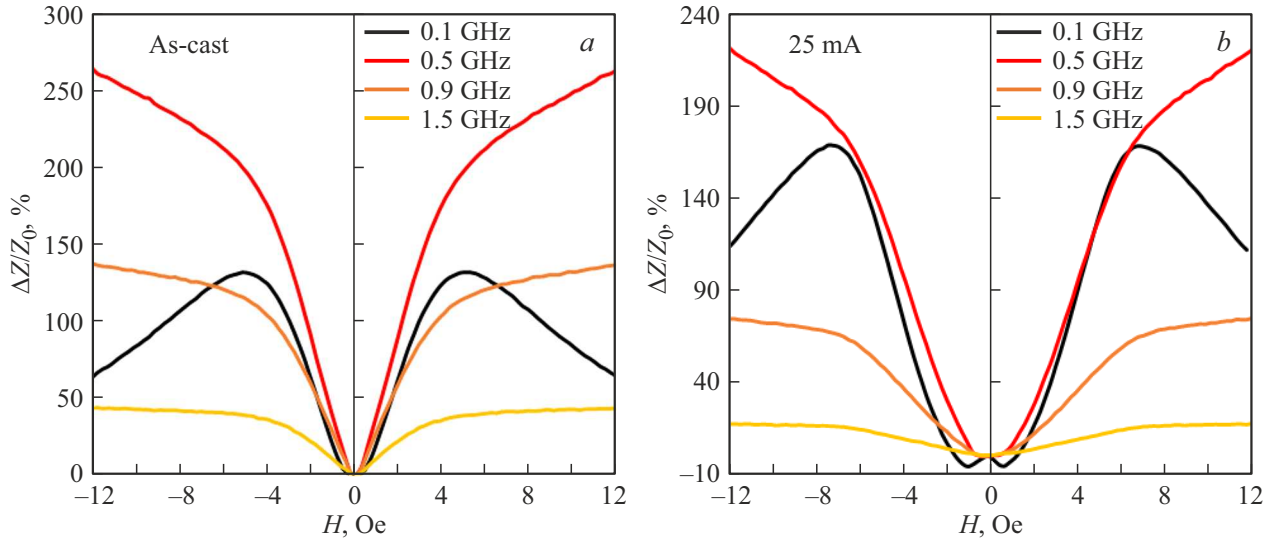

Figure 3. Relative impedance change $\Delta Z/Z_0$ at room temperature for $Co_{27.4}Fe_5B_{12.26}Si_{12.26}Ni_{43.08}$ microwire for various frequencies: *a* — in initial condition, *b* — after annealing at 25 mA.

At the approach to T_C, anisotropy constant K (or magnetostriction constant λ_s) decreases faster than magnetization. For traditional anisotropy model for localized spin system in a wide temperature range $K(T) \propto M_s^{l(l+1)/2}$, where l is the spherical harmonic order defining the angular dependence of local anisotropy. In close vicinity to T_C $K(T) \propto M_s^l$ [23]. For uniaxial materials $l = 2$. The theory adequately describes the anisotropy and magnetostriction behavior in magnetic dielectrics and is also applicable to amorphous transition metal alloys [24]. Therefore, it is assumed that the anisotropy constant caused by magnetostriction varies with temperature as

$$K \propto M_s^n, \quad n = 2{-}3. \tag{1}$$

This explains quick reduction of the circular anisotropy field. And the role of shape anisotropy increases and leads to the increase in the residual magnetization.

3.2. MI characteristics for various frequencies

Relative impedance variation (MI parameter) was calculated as

$$\frac{\Delta Z}{Z_0} = \frac{Z(H) - Z(H=0)}{Z(H=0)}. \tag{2}$$

$\Delta Z/Z_0$-characteristics for various frequencies are shown in Figure 3. The behavior is typical of the materials with easy magnetization axis perpendicular to the magnetic field. For further discussion, some theoretical findings for

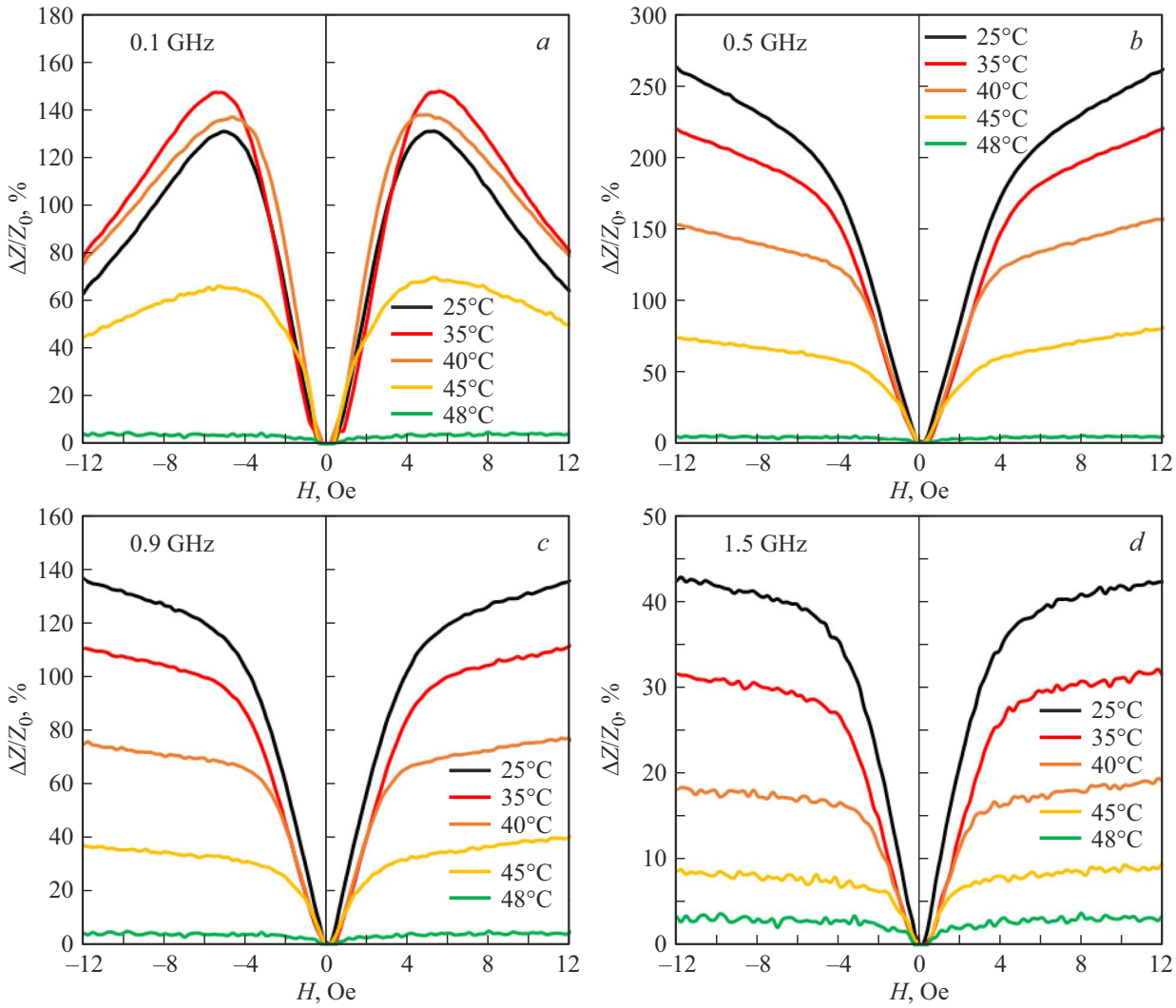

Figure 4. Relative impedance variation $\Delta Z/Z_0$ for various temperatures and frequencies for $Co_{27.4}Fe_5B_{12.26}Si_{12.26}Ni_{43.08}$ microwire: *a* — 0.1, *b* — 0.5, *c* — 0.9, *d* — 1.5 GHz.

high-frequency impedance of microwire materials will be presented. When a strong skin effect is assumed, i.e. skin layer depth is lower than the wire radius a, impedance Z is expressed as follows [25]:

$$Z = R_{DC}\frac{(1-j)a}{2\delta}\left(\sqrt{\mu}\cos^2\theta + \sin^2\theta\right). \qquad (3)$$

In equation (3), R_{DC} is the DC resistance, δ corresponds to the skin layer depth of a nonmagnetic metal ($\mu = 1$), μ is the dynamic permeability and θ is the static magnetization deviation angle from the wire axis. The dynamic permeability in equation (3) is calculated as follows:

$$\mu = 1 + \frac{\Omega_M(\Omega_1 - i\tau\omega)}{(\Omega_1 - j\tau\omega)(\Omega_2 - j\tau\omega) - \omega^2}, \qquad (4)$$

$$\Omega_M = \gamma 4\pi M_s,$$

$$\Omega_1 = \gamma\left(H\cos\theta + H_K\cos^2(\alpha-\theta)\right) + \Omega_M,$$

$$\Omega_2 = \gamma\left(H\cos\theta + H_K\cos 2(\alpha-\theta)\right).$$

In equation (4), α is the angle between the easy anisotropy axis and wire axis, H is the external magnetic field directed along the wire axis, $H_K = 2K/M_s$ is the anisotropy field, ω is the angular frequency, τ is the relaxation parameter and γ is the gyromagnetic ratio. At low frequencies

$$\mu \approx 1 + \frac{4\pi M_s}{H\cos\theta + H_K\cos 2(\alpha-\theta)}, \qquad (5)$$

whose value at $\alpha \approx \pi/2$ is maximum at $H \approx H_K$ and provides the impedance peak at low frequencies. When the frequency increases, the peak widens and shifts towards a higher field area. At 0.1 GHz, two symmetrical peaks are observed in fields $\pm H_m$, but H_m is considerably higher than H_K determined from the hysteresis loops. This may be also due to surface anisotropy features. For higher frequencies, perceptible impedance variations are associated with the variation of static magnetization angle θ under magnetic field. When the wire has been magnetized along the axis (in (3) $\cos^2\theta = 1$), all Z variations are

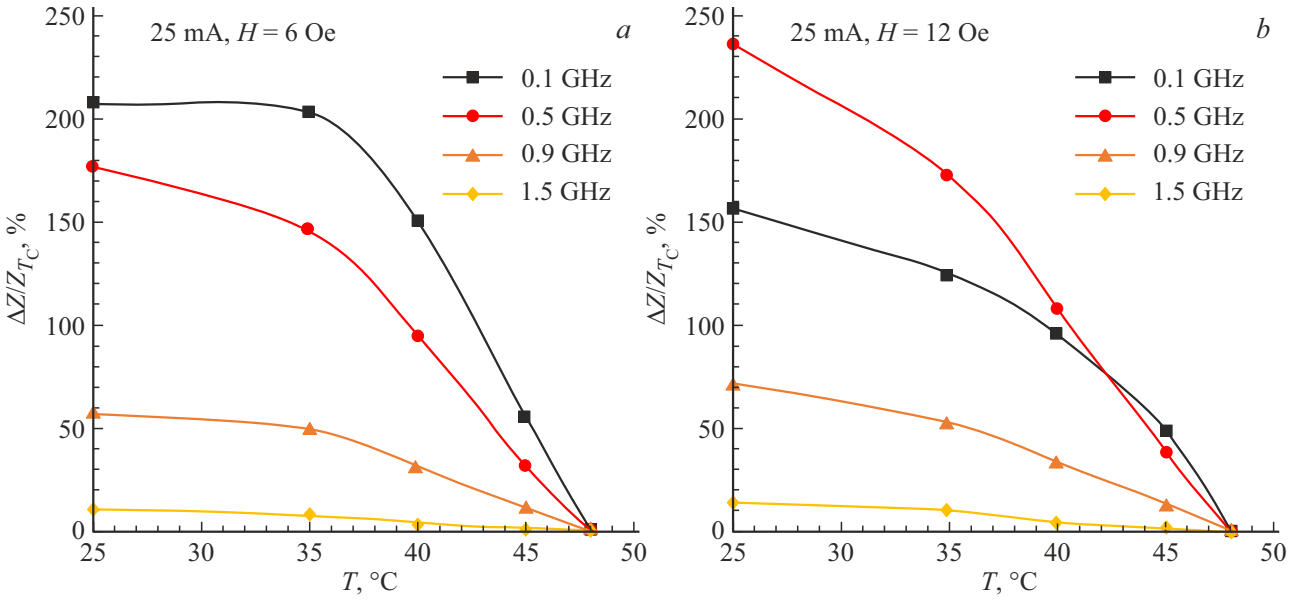

Figure 5. Relative impedance variation vs. temperature $\Delta Z/Z_{T_C}$ for different frequencies for $Co_{27.4}Fe_5B_{12.26}Si_{12.26}Ni_{43.08}$ microwire. Results for two fields are shown: *a* — 6, *b* — 12 Oe.

associated with permeability dispersion μ, which has weak dependence on H away from the ferromagnetic resonance. In this case, the impedance increases with much lower slope and an inflection point occurs in curve $Z(H)$. At higher frequencies (higher than ferromagnetic resonance frequency $\omega \gg \omega_{res} = \sqrt{\Omega_1 \Omega_2}$) and low fields, the impedance achieves saturation. For this type of wires, such high-frequency impedance characteristics were demonstrated in [22,26,27].

3.3. Temperature influence on MI with variation from room temperature up to T_C (T-MI)

Considerable variations of magnetic parameters at the approach to T_C will cause changes in MI behavior. Figure 4 shows field dependences $\Delta Z/Z_0$ for different temperatures (up to T_C) at different frequencies from 0.1 to 1.5 GHz for the initial microwire. MI behavior with temperature increase is maintained at all frequencies. In the low field area, where $\cos^2\theta \ll 1$, impedance variation with temperature is negligible, since the impedance has weak dependence on magnetic properties. At low frequencies, maximum variations are observed in the field where the impedance achieves its peak, and $\Delta Z/Z_0$ has nonmonotonic dependence on temperature: slight increase is observed at first followed by drop. This may be attributable to the increase in initial susceptibility (in (1) $n > 2$). With increase in frequency, MI for fields $H > H_K$ steadily decreases with increase in temperature. At the approach to T_C, ferromagnetic resonance frequency decreases ($\omega_{res} \to \gamma H$ at $T \to T_C$). This means that with the temperature increase, permeability will decrease rapidly, since for any frequency $\omega > \gamma H$ and temperatures which are close to T_C, the condition $\omega > \omega_{res}(T)$ will be met. Thus, impedance decrease is observed. Maximum MI variation with temperature is observed at 0.5 GHz. For example, in field 12 Oe $\Delta Z/Z_0$ decreases from 275 to 75% with temperature variation from room temperature up to 45°C and almost vanishes (lower than 2%) at $T = 48$°C. Considerable impedance variations are also preserved at higher frequencies — 42% at 1.5 GHz.

Similar behavior was also obtained for the annealed microwire. This means that partial relaxation of internal stresses does not influence the magnetic structure and the high-frequency impedance variations are associated with the approach to T_C. Figure 5 shows relative impedance variation vs. temperature for the annealed wire specified for the relative impedance variation at $T \approx T_C$ (48°C):

$$\frac{\Delta Z}{Z_{T_C}} = \frac{Z(H,T) - Z(T_C)}{Z(T_C)}.$$

Since at low fields, the impedance variations with temperature are negligible, temperature behavior of the impedance under magnetic field is addressed below. The data is provided for two fields: H_m, where impedance as a function of filed has its peak at low frequencies, and 12 Oe maximum field used for the experiment (since impedance increase with field is observed at high frequencies). At low frequencies in field H_m, $\Delta Z/Z_{T_C}$ is at plateau and starts decreasing at $T > 35$°C (by 210% at $T = T_C$). With frequency increase, impedance-temperature variations become lower and are about 12% at 1.5 GHz. In 12 Oe field, the parameter $\Delta Z/Z_{T_C}$ is maximum at 0.5 GHz and is equal to 240% due to the absence of peak on the impedance-field dependence. However, with further frequency increase, $\Delta Z/Z_{T_C}$ also decreases rapidly to 16% at 1.5 GHz. It should be noted that for the annealed wire, impedance-temperature variations are higher at low frequencies compared with

the initial specimen, which may be attributed to lower anisotropy near the surface due to stress relaxation. This is also the reason why the impedance variations at higher frequencies are considerably lower.

4. Conclusion

Magnetoimpedance(MI)-temperature behavior was investigated in $Co_{27.4}Fe_5B_{12.26}Si_{12.26}Ni_{43.08}$ microwires ($T_C \approx 48^\circ C$) with negative magnetostriction and circular magnetic anisotropy. The findings show that relative impedance variation with temperature increase from room temperature to T_C is high up to GHz frequencies ($\sim 70-140\%$), and depends on the magnetic field influence. Temperature MI may be of interest for fabrication of microwave proximity temperature sensors.

Acknowledgments

The authors would like to express gratitude to V. Larin, MFTI Ltd (http://www.microwires.com), for provision of microwire specimens.

Funding

The study was supported by the RFBR grant No. 20-32-90129.

Conflict of interest

The authors declare that they have no conflict of interest.

References

[1] G. Herzer. Acta Materialia **61**, *3*, 718 (2013).
[2] P.R. Ohodnicki Jr, Y.L. Qin, D.E. Laughlin, M.E. McHenry, V. Keylin. J. Magn. Magn. Mater. **322**, *3*, 315 (2010).
[3] W.P. Tian, H.W. Yang, S.D. Zhang. Acta Metallurgica Sinica (Engl. Lett). **31**, *3*, 308 (2018).
[4] G.V. Kurlyandskaya, N.G. Bebenin, V.O. Vas'kovsky. Fizika metallov i metallovedenie **111**, *2*, 136 (2011) (in Russian).
[5] L. Kraus, Z. Frait, K.R. Pirota, H. Chiriac. J. Magn. Magn. Mater. **254**–**255**, 399 (2003).
[6] J. Nabias, A. Asfour, J.-P. Yonnet. IEEE Trans. Magn. **53**, *4*, 4001005 (2017).
[7] M. Malátek, P. Ripka, L. Kraus. Sens. Actuators A Phys. **147**, *2*, 415 (2008).
[8] A. Chizhik, A. Stupakiewicz, A. Maziewski, A. Zhukov, J. Gonzalez. J. Magn. Magn. Mater. **400**, 356 (2016).
[9] L.V. Panina, A. Dzhumazoda, S.A. Evstigneeva, A.M. Adam, A.T. Morchenko, N.A. Yudanov, V.G. Kostishyn. J. Magn. Magn. Mater. **459**, 147 (2018).
[10] R. Varga, P. Klein, R. Sabol, K. Richter, R. Hudak, I. Polaček, D. Praslicka, M. Šmelko, J. Hudak, I. Mikita, G.A. Badini-Confalonieri, R. El Kammouni, M. Vázquez. Springer Ser. Mater. Sci. **252**, 169 (2017).
[11] H. Chiriac, C.S. Marinescu, T.-A. Óvári. J. Magn. Magn. Mater. **196**–**197**, 162 (1999).
[12] A.V. Semirov, M.S. Derevyanko, D.A. Bukreev, A.A. Moiseev, G.V. Kurlyandskaya. Tech. Phys. **58**, *5*, 774 (2013).
[13] M. Kurniawan, R.K. Roy, A.K. Panda, D.W. Greve, P. Ohodnicki, M.E. McHenry. J. Electron. Mater. **43**, 4576 (2014).
[14] D.A. Bukreev, A.A. Moiseev, M.S. Derevyanko, A.V. Semirov. Russ. Phys. J. **58**, 141 (2015).
[15] V. Zhukova, M. Ipatov, A. Zhukov, R. Varga, A. Torcunov, J. Gonzalez, J.M. Blanco. J. Magn. Magn. Mater. **300**, *1*, 16 (2006).
[16] S. Partha, A. Basu Mallick, R.K. Roy, A.K. Panda, A. Mitra. J. Magn. Magn. Mater. **324**, *8*, 1551 (2012).
[17] H. Chiriac. Mater. Sci. Eng. A **304**–**306**, *1*, 166 (2001).
[18] M. Churyukanova, V. Semenkova, S. Kaloshkin, E. Shuvaeva, S. Gudoshnikov, V. Zhukova, I. Shchetinin, A. Zhukov. Phys. Status Solidi A **213**, *2*, 363 (2016).
[19] A. Chizhik, A. Stupakiewicz, V. Zablotskii, M. Tekielak, V. Stupakevich, A. Zhukov, J. Gonzalez, A. Maziewski. J. Alloys. Compounds **632**, 520 (2015).
[20] M.G. Nematov, I. Baraban, N.A. Yudanov, V. Rodionova, F.X. Qin, H.-X. Peng, L.V. Panina. J. Alloys. Compounds **837**, 155584 (2020).
[21] Y. Zhao, Y. Wang, D. Estevez, F.X. Qin, H. Wang, X.F. Zheng, D. Makhnovskiy, H.X. Peng. Measurement Sci. Technol. **31**, *2*, 025901 (2019).
[22] J. Alam, M. Nematov, N. Yudanov, S. Podgornaya, L. Panina. Nanomater. **11**, *5*, 1208 (2021).
[23] H.B. Callen, E. Callen. J. Phys. Chem. Solids **27**, *8*, 1271 (1966).
[24] R.C. O'Handley. Phys. Rev. B **18**, *2*, 930 (1978).
[25] D.P. Makhnovskiy, L.V. Panina, D.J. Mapps. Phys. Rev. B **63**, *14*, 144424 (2001).
[26] P. Marín, D. Cortina, A. Hernando. J. Magn. Magn. Mater. **290**–**291**, *Part 2*, 1597 (2005).
[27] M. Vázquez, A.-L. Adenot-Engelvin. J. Magn. Magn. Mater. **321**, *14*, 2066 (2009).

Translated by Ego Translating